Effects of applied magnetic field on IPG6-S, test-bed for an ABEP-based inductive plasma thruster (IPT)

Francesco Romano [1], Georg Herdrich [1], Tilman Binder [1], Adam Boxberger [1], Constantin Traub [1], Stefanos Fasoulas [1], Tony Schönherr [2], Peter Roberts [3], Kate Smith [3], Steve Edmondson [3], Sarah Haigh [3], Nicholas Crisp [3], Vitor Toshiyuki Abrao Oiko [3], Rachel Lyons [3], Stephen D. Worrall [3], Sabrina Livadiotti [3], Jonathan Becedas [4], Gerardo Gonzalez [4], Rosa Maria Dominguez [4], Leonardo Ghizoni [5], Victor Jungnell [5], Kristian Bay [5], Jonas Morsbøl [5], Daniel Garcia-Almiñana [6], Silvia Rodriguez-Donaire [6], Miquel Sureda [6], Dhiren Kataria [7], Ron Outlaw [8], Rachel Villain [9], Jose Santiago Perez [9], Alexis Conte [9], Badia Belkouchi [9], Ameli Schwalber [10], Barbara Heißerer [10]

[1] Institute of Space Systems (IRS), University of Stuttgart, Pfaffenwaldring 29, 70569, Stuttgart, Germany, romano@irs.uni-stuttgart.de

[2] ESA/ESTEC, Keplerlaan 1, 2201 AZ Noordwijk, The Netherlands, tony.schoenherr@esa.int

[3] School of Mechanical, Aerospace and Civil Engineering, The University of Manchester, George Begg Building, Sackville Street, Manchester, M13 9PL, UK.

[4] Elecnor Deimos Satellite Systems, C/ Francia 9, 13500, Puertollano, Spain

[5] GomSpace AS, Alfred Nobels Vej, 21A 1., Denmark

[6] UPC-BarcelonaTECH, Colom 11, TR5 - 08222 Terrassa, Spain

[7] Mullard Space Science Laboratory, University College London, Holmbury St. Mary, Dorking, Surrey, RH5 6NT, UK

[8] Christopher Newport University, Newport News, Virginia 23606, US

[9] Euroconsult, 86 Boulevard de Sébastopol, Paris, France

[10] concentris research mamagement gmbh, Ludwigstrasse 4, 82256 Fürstenfeldbruck, Germany

KEYWORDS

Atmosphere-Breathing Electric Propulsion - ABEP - RAM-EP - VLEO - Inductive Plasma Thruster - IPT

ABSTRACT

An atmosphere-breathing electric propulsion system (ABEP) [1] captures the residual atmosphere of a planet and uses it as propellant for an electric thruster to counteract the drag. The system would theoretically allow orbiting for unlimited time without on-board propellant storage. A new range of altitudes, e.g. 120-250 km in Earth orbit, the Very-Low Earth orbit (VLEO), for permanent orbiting can be accessed, thereby enabling new scientific missions. ABEP can be conceptually applied to any planet with atmosphere. IRS has several decades of heritage on the development of inductively heated plasma generators (IPG) [2] [3]. Such devices are electrodeless, removing the issue of electrode erosion that reduces performance over time (see RIT, HET). Aggressive gases such as O as propellant, highly present in VLEO, will cause even faster erosion. IRS is currently developing an inductive plasma thruster (IPT) for ABEP application within the H2020 DISCOVERER project [4].

1 ATMOSPHERE-BREATHING ELECTRIC PROPULSION

VLEO is a very interesting altitude range for many scientific, civil, and military purposes. ESA's mission GOCE ended in 2013; it provided detailed information of the Earth's geomagnetic field by orbiting as low as 229 km [5] using GIT to compensate the drag. The amount of propellant on board has been the limiting lifetime factor for the mission. If conventional propulsion is used, drag is also a limiting factor in terms of costs, as this translates in an increased amount of propellant to be carried on-board, leading to high total payload mass. The lifetime of a S/C orbiting in LEO can be increased significantly by applying an efficient propulsion system that compensates the drag. The basic idea of an ABEP is of using the residual atmosphere as propellant to generate thrust. This will decrease, ideally nullify, the on board propellant requirement and will partially or fully compensate the drag, for finally allow continuous operation of a S/C in VLEO. A conceptual scheme of a S/C with ABEP

is shown in Fig. 1.

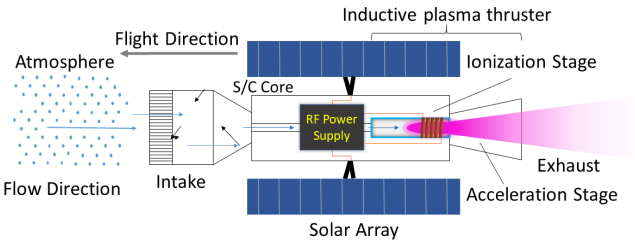

Figure 1: ABEP Concept [1].

2 IPG6-S Facility

The candidate test-bed ABEP IPT is IPG6-S. This is a smaller scale IPG compared to the ones available at IRS, in terms of discharge channel size and power level. The main advantage of such a device is its electrode-less design. No critical components are in direct contact with the plasma, therefore any issues concerning erosion are eliminated. In addition, IPG do not employ a grid system that could suffer from erosion. The IPG functional principle enables ignition also at very low densities. The plasma leaving the discharge channel is already neutral, removing the issue of designing a neutralizer operating on atmospheric propellant. These characteristics are even more important as the atmospheric propellant for VLEO application, will be mostly N_2, O, and O_2 [1], the latter two highly chemically aggressive for things such as electrodes and grids. The advantages as propulsion system, are can be summed up:

- Electrode-less design, no accelerating grids;
- No neutralizer needed, plasma already neutral;
- Less sensitive in terms of minimum pressure and mass flow for ignition.

IPG6-S, see Fig. 2 has been chosen for its size and power levels that are scalable to a small S/C [1]. The facility of IPG6-S is provided with the following subsystems:

- Vacuum;
- Power supply;
- Gas supply;
- Water cooling.

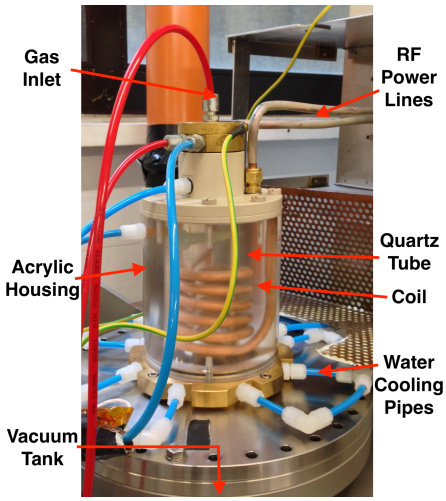

Figure 2: IPG6-S

The facility at its whole is shown within the schematics in Fig. 3.

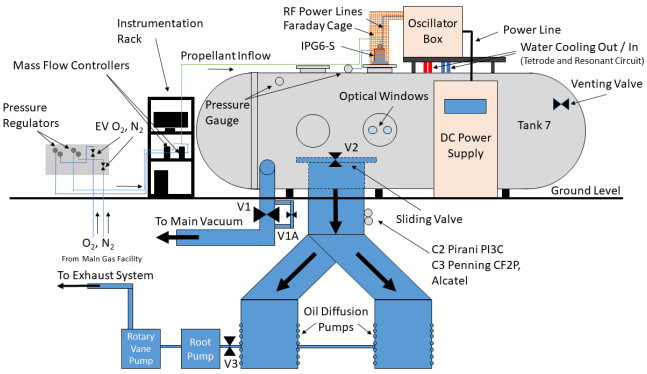

Figure 3: IPG6-S Facility Scheme

2.1 IPG6-S

IPG6-S, see Fig. 2, is composed by a discharge channel made of quartz with an internal diameter of $\phi_{int.} = 37\,\text{mm}$, and a length of $180\,\text{mm}$. A 5.5-turn internally water cooled copper coil is wrapped around the discharge channel. The top injector head, the bottom flange, and the de Laval nozzle are made of brass, all of them are water cooled. The IPG6-S housing is made of acrylic and holds together the structure. The de Laval nozzle has a modular design [6] and is currently with a throat diameter of $20\,\text{mm}$, and an outlet diameter of $40\,\text{mm}$.

2.2 Vacuum Subsystem

The vacuum chamber, named Tank 7, has a cylindrical shape, with a length of 4.8 m and a diameter of 2 m. The vacuum chamber is connected to the central IRS vacuum facility, on the side. The central vacuum facility can provide a total pumping speed of more than $250\,000\,\mathrm{m}^3/\mathrm{h}$. An additional system of two oil diffusion pumps is dedicated only to this vacuum chamber, directly connected at the bottom of it. Each of the oil diffusion pump provides $50\,000\,\mathrm{L/s}$ of suction rate, enabling a final minimum background pressure of 8×10^{-4} Pa without mass flow. The initial testing phase of IPG6-S on the refurbished facility has been possible only with the central vacuum facility. IPG6-S is mounted on a flange on the top of the vacuum chamber directing the plasma downwards. The sliding valve V2 made of aluminum is protected from the plasma jet by a graphite shield. Pressure is measured by two Pfeiffer PKR 251 Full-Range gauges, one for the vacuum chamber, and one at the injector head of IPG6-S. With the main vacuum system, a base pressure of < 1 Pa is achieved. Currently, with the maximum mass flow of $> 26.35\,\mathrm{mg/s}$ applied to IPG6-S, the vacuum chamber pressure does not increase above 1.6 Pa.

2.3 Power Supply

The electrical power is provided by the RF generator Himmelwerk HGL 20-4B, that provides a maximum of 20 kW power at a frequency of $\sim$ 4 MHz, dependent on the impedance of IPG6-S. It is composed of two main elements, the first is the high voltage DC power supply, air-cooled, located on the side of the vacuum chamber, and the second is the oscillator that produces the RF signal for IPG6-S, located on the top of the vacuum chamber close to IPG6-S. The oscillator is provided with a tetrode and the resonant circuit that includes the IPG6-S coil, both of them are water cooled. The high voltage DC power supply receives the three phase energy from the grid, raises its voltage with a transformer and by a rectifier produces a DC high voltage of $7.7, 8.2, 8.5$ kV, that directly feeds the tetrode in the oscillator. In parallel a voltage between -150 and 200 V is delivered to the triode in the power supply, the latter serves to produce the DC voltage from 0 to 1700 V that regulates the screen grid of the tetrode in the oscillator. The higher the applied screen grid voltage is, the larger is the current allowed to flow through the tetrode, with a maximum of $I_A = 4$ A. The output current flows through the resonant circuit that determines, together with the IPG6-S coil, the operating frequency, in the current configuration at 3.3 MHz. At the power supply anode current I_A that flows through the tetrode is shown together with the screen voltage. The third analog displays shows the active power $P_{RF,active}$ that is finally delivered, it is the regulated value of the power supply. Anode current and active power measurements have been connected to the datascan to provide more precise and reliable values for comparison.

2.4 Gas Supply Subsystem

The gas supply subsystem is composed by two pressure regulators connected to the main gas facility of the IRS laboratory, and two mass flow controllers - MFC. The system is flexible such that can work with the main gas facility, or autonomously with single gas bottles. The current available gases are N_2 and O_2. The gas flow is provided by two Tylan FC-2900, one for each gas, The facility can run with either one of the two gas, or with a mixture. The total maximum mass flows reached by the two flow controllers operating together is, in the current configuration of $26.35\,\mathrm{mg/s}$. An additional Bronkhost F-201CV MFC has been placed for higher N_2 mass flow testing.

2.5 Water Cooling Subsystem

The water subsystem is required to remove the heat from many components that during operation are heated up by the electrical power. Water is feed through the system by two water pumps. One pump provides independent cooling for the tetrode of the power supply. The second one provides water for the cooling of the IPG6-S quartz tube, the injector, the nozzle, the cavity calorimeter, and the resonant circuit that includes the IPG6-S coil. A panel of manual water valves is available, water flow is currently measured at the calorimeter inflow, generator outflow, and resonant circuit outflow (that includes the coil cooling). Water flow has been

measured for the cooling of the tetrode and is used as fixed value since there is no valve controlling it. Water temperature is measured by Pt100 located at different points on the circuit. At the main inlet the reference temperature is taken. Moreover, Pt100 are place at each water outflow line, as close as possible to the heat source, so that the cooling power balance can be monitored. Pt100 close to the IPG6-S have been placed outside of the Faraday cage to avoid unwanted RF-coupling. For the calorimeter, the Pt100 is located inside the vacuum chamber, close to the calorimeter. The water cooling subsystem is shown within Fig. 4.

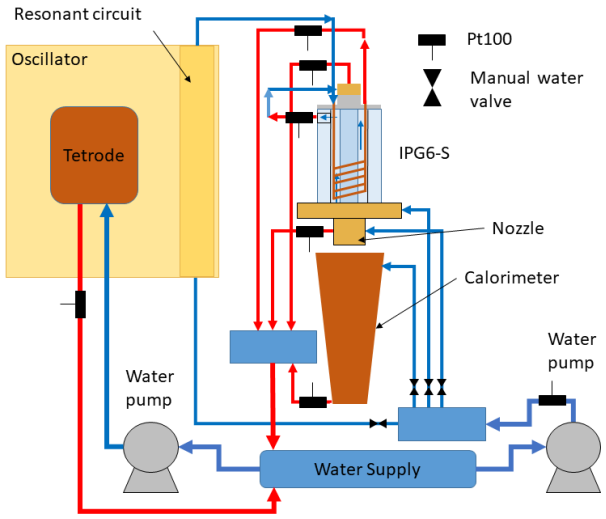

Figure 4: Water Cooling Subsystem Scheme

The water temperatures are used to estimated the heating powers of the different components of the facility as in Eq. 1.

$$P_i = \dot{m}_{w,i} C_{p,w} (T_{warm,i} - T_{cold,i}) \qquad (1)$$

Where $\dot{m}_{w,i}$ is the water flow in the desired section i, $C_{p,w}$ is the specific heat of water at 20 °C, and $T_{warm,i}$, $T_{cold,i}$ are the water temperatures.

3 Power Balance

Testing of IPG6-S have been performed to evaluate the power balance of the facility after the recent refurbishment [1]. The testing procedure consisted in a setting of mass flows of propellant, and to apply different active power levels $P_{RF,active}$. Preliminary results are shown for 20 mg/s propellant flow of N_2 in Fig. 5 and with O_2 as working gas, see Fig 6. To the mass flow corresponds a discharge channel pressure p_{disch}, that increases as the applied power is incremented, this is shown within Fig. 7, where, for example, $p_{disch} = 45.53 - 76.44$ Pa. $P_{RF,active}$ is quite noisy during operation, and it might be the sign of interference and/or high power reflection from the plasma back into the power supply. An interesting condition has been observed while operating with O_2 at 4.63 mg/s, corresponding to $p_{disch} = 21.78 - 22.22$ Pa. The signal from $P_{RF,active}$, see Fig. 6, and 8, has the least noise when compared to all the others tests, which may suggests that there is an optimum condition for the minimized reflected power for a given p_{disch} and I_A and $P_{RF,active}$, this requires further testing.

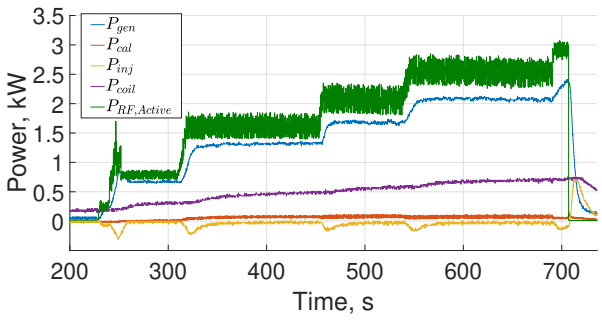

Figure 5: IPG6-S Power Balance for 20 mg/s N_2

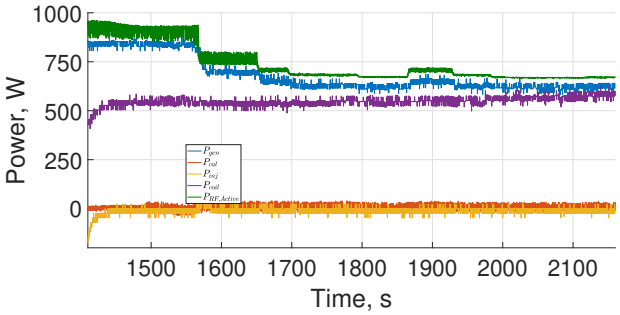

Figure 6: IPG6-S Power Balance for 4.36 mg/s O_2

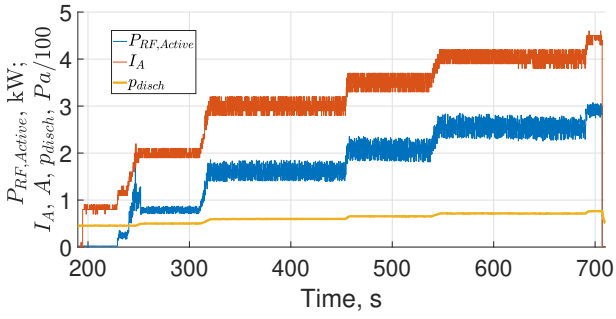

Figure 7: IPG6-S Power vs Current vs Pressure Discharge Channel, for 20 mg/s N_2

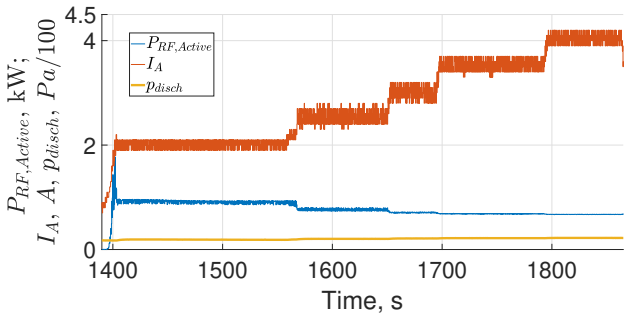

Figure 8: IPG6-S Power vs Current vs Pressure Discharge Channel, for 4.36 mg/s O_2

From the precedent plots can be clearly seen that the power measured by the calorimeter is very low, < 100 W for most of the cases, translating in a very low coupling efficiency η_{couple} of the electric power into the jet power. η_{couple}, see Eq. 2, is 30% for most of the testing conditions at $\dot{m}_{N_2} = 20 - 200$ mg/s, and at $\dot{m}_{O_2} = 4.63$ mg/s.

$$\eta_{couple} = \frac{P_{gen} + P_{cal}}{P_{RF,active}} \tag{2}$$

4 INDUCTIVELY HEATED PLASMA THRUSTER

Within the EU-funded DISCOVERER project, the IRS aim is to develop an intake and a thruster for an ABEP system. The thruster, the IPT, has to operate in the operational conditions given by the intake design in terms of collected propellant and pressure at the thruster. The power requirement is set between $0.5 - 5$ kW. Since a major design is necessary to create an efficient plasma source and, second, an efficient acceleration stage for the plasma, we have chosen to investigate the design an efficient plasma source considering most of the major parameters free, included considering a new power supply. Huge research has been done in the past over IPG, ICP and ionization sources that take advantage of Helicon waves, in particular the very late research from Francis Chen [7], [8] proposed very optimized designs of plasma sources with respective description of the influencing parameters. For the optimization procedure the software tool HELIC has been utilized, it is based on the work of Arnush and Chen [9], [10], [11] able to calculate plasma parameters such as the wave variables, the power spectra, and the resistive loading. This is aimed to help the designing RF plasma sources and experiments, and serves only as initial evaluation of the plasma properties.

4.1 HELIC Description

A complete description of the HELIC tool can be found in the theory developed by Chen and Arnush [9], [10], [11], here a briefly explanation will be presented. HELIC is a software written in C++. It resolves four coupled differential equation for each wave number k along the axis of symmetry of the plasma cylinder z. These are Maxwell's equation for a radially uniform plasma with standard cold-plasma dielectric elements, that are manipulated to be in the form for the Fourier transformed variables. Two different waves are obtained that are later combined together by applying algebraically the boundary conditions. The geometry of the HELIC software tool is shown in Fig. 9.

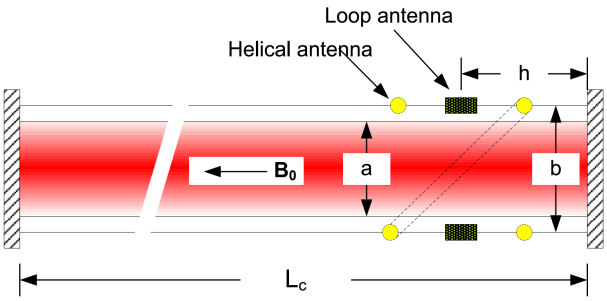

Figure 9: HELIC Geometry

The restriction are the followings:

- the applied DC magnetic field has to be uniform;
- plasma creation and transport are not considered;
- plasma is assumed to have cylindrical symmetry.

The magnetic field strength B_0, plasma density n, electron temperature T_e, and neutral pressure $p_0(r)$ are given as input to the tool. The antenna is considered as an infinitely thin sheet at $r = b$ that carries the a sheet current where its divergence

is 0. The antenna type can be chosen, and to each shape it correspond an azimuthal mode number m. HELIC accounts for electron-neutral and electron-ion collisions, arbitrary radial profile of n, T_e, and $p_0(r)$, reflections from end boundaries, arbitrary antenna shape, displace current, and finite ions and electron masses (fundamental for the Trivelpiece-Gould mode). According to [7], the rate of deposition of the RF energy, depends on the loading resistance R_P at the output of the matching network. To achieve most of the power to be deposited into the plasma, as R_P is proportional to the deposition of RF energy into the plasma, is that R_P must be much larger than R_C, which is the resistance of the circuit. In small discharge tubes, R_P tends to be too low, $< 1\,\Omega$, unless it is made use of the low-field peak of R_P over n. The power that is actually reaching the plasma is as according to Eq. 3.

$$P_{in} = P_{RF}\frac{R_P}{R_P + R_C} \tag{3}$$

Finally, as the parameters are normalized to a current of 1 A. The first design approach is to look at $R_P >> 1\,\Omega$ as a function of B_0, f_0, a, b, and antenna shape, over a given plasma density range that is interesting for propulsion purposes.

4.2 HELIC Input Parameters

Proper choice of input parameters is fundamental for reliable results, therefore this subsection is dedicated to the parameters choice. First, T_e, $p_0(r)$, have been set to the standard values suggested by Chen [7] of $T_e = 3$ eV, and $p_{g0} = 105$ mTorr $= 1.33$ Pa. Radial steps N have been set to 99 according to the instructions for more resolution. The cavity type has been set to "bounded", so that its size and shape will determine the range of k of the waves. Parameters not mentioned in this section have been kept to default. To be kept in mind that length, radius are to be given in meter, B_0 in Gauss, n in cm^{-3}, f_0 in Hz, and pressure in mTorr.

4.2.1 Plasma, Antenna & Cavity Radii

Three different sizes have been set for the simulations to see their influence, in particular a is the plasma radius that has been assumed equal to the internal diameter of the discharge channel ϕ of $\phi = 2a = 18.5,\ 37,\ 74$ mm, where the discharge channel thickness $t_{dc} = 1.5$ mm. b is the radius of the antenna, the distance from the axis at which the current is flowing. At first approximation $b = a + t_{dc} + 1.5\,\mathrm{mm} = a + 3\,\mathrm{mm}$. c is the radius of a bounding conductive cylinder set to 0.2 m so that $c >> b$ to make the results insensitive to it.

4.2.2 Ion, Frequency, Azimuthal Mode

Ar has been set at working gas. f_0 is the frequency, this has been set to 3.3 (current IPG6-S configuration), 13.56, 27.12, and 40.68 MHz. Wave number m depends on the antenna that is used.

4.2.3 Antenna Type

An antenna shape similar to that of IPG6-S has been chosen, a t-turn Helix $m = 1$ with 5 turns (no half turns are possible as input), and a length of 80 mm. A Half Helix had also been tested, with a length of $L_A = 75$ mm but provided significantly lower performances for the given geometries, and, finally a 1-Loop $m = 0$ antenna according to Chen suggestions [8], but since for our application $P < 5$ kW, we opted for more turns coil.

4.2.4 Cavity length, Image sign, Antenna distance from center

The cavity length has been set to 2 m such that ejection of the plasma is simulated by giving a very long cavity, see 9. The image sign has been tested both to be $+1$ and -1 so to simulate the eventual discharge improvement by placing a conductive rather than an insulating top plate. A conductive one should, under certain conditions, provide constructive wave reflection and increase R_P. The antenna distance from the center ZA has been in first simulations set to 0, in the latest it has been moved to the current IPG6-S-like configuration, considering the same antenna length.

4.2.5 Plasma Density, Magnetic Field, Plasma Density Profile

A plasma density range has been estimated starting from the intake performances [12], [13], [14], given that this can be highly enhanced by the use of specular reflecting surfaces, and from electrodeless thruster literature that locates the value of the plasma density between $10^{18}-10^{19}\,\mathrm{m}^{-3}$, this range has been however extended to provide a broader view of the plasma behavior. Multiple software runs showed a magnetic field between 0.02 and $0.5\,\mathrm{T}$ to provide the required performance in terms of R_P. Very small values of B_0 can be used to simulate ICP performance. The plasma density profile has been tested uniform and, later, with a plasma profile that has a peak in the symmetry axis z such that $s = 2$, $t = 4$, and $f_a = 0.1$ [7].

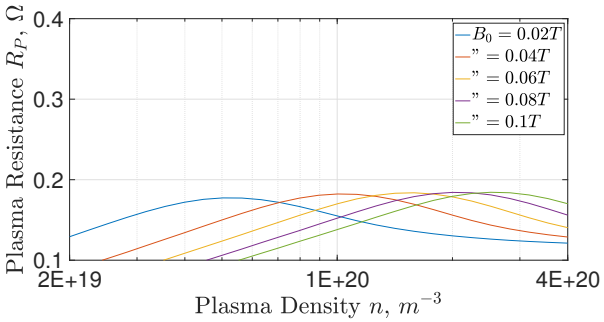

Figure 10: R_P vs n vs B_0, Insulating Top Plate. $\phi = 2a = 18.5\,\mathrm{mm}$, $f = 3.3\,\mathrm{MHz}$.

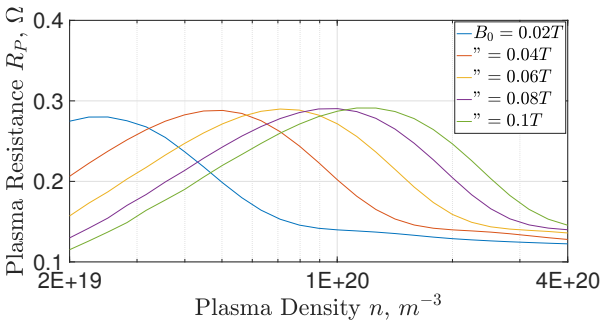

Figure 11: R_P vs n vs B_0, Insulating Top Plate. $\phi = 2a = 37\,\mathrm{mm}$, $f = 3.3\,\mathrm{MHz}$.

5 HELIC Results

The HELIC results of R_P over n, B_0, f_0, a are presented in this section. Usually, a R_P vs n curve has a peak, the so-called low-peak field, for a given $B_=$ and n, which should be the best point for that condition for good operation. The first simulations show that for larger diameters $\phi = 2a$ or higher frequencies f_0 the peak shifts to lower n but the overall R_P is higher. Concerning the diameter, this is most probably due to the chosen uniform plasma density profile. The magnetic field B_0 strength is shown to increase R_P and move the peak to higher plasma densities n. Variation of discharge channel diameter $\phi = 2a$, together with a sweep of $B_0 = 0.02 - 0.1\,\mathrm{T}$ is shown in Fig. 10, 11, and 12 for $f_0 = 3.3\,\mathrm{MHz}$ that of the IPG6-S current facility set-up, the antenna is a half-helical of $7.5\,\mathrm{cm}$ of length. The effect is to increase R_P but the P_{RF} required might be too high to fill the entire discharge channel [15]. Moreover, the position of the low-field peak is influenced by the position and length of the antenna.

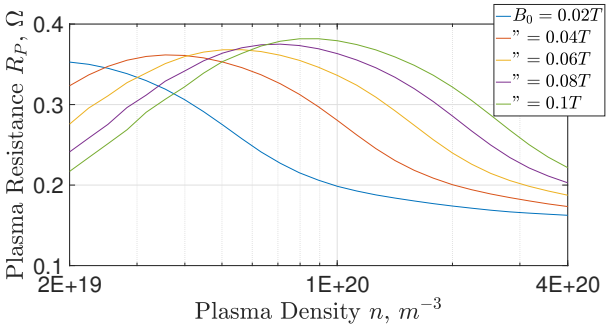

Figure 12: R_P vs n vs B_0, Insulating Top Plate. $\phi = 2a = 74\,\mathrm{mm}$, $f = 3.3\,\mathrm{MHz}$.

In Fig. 13 the effect of the variation of different f_0 is shown for an applied $B_0 = 0.0015\,\mathrm{T}$ to simulate an ICP discharge. For the given n range, discharge channel, antenna geometry, an increase in f_0 leads to an increase in R_P.

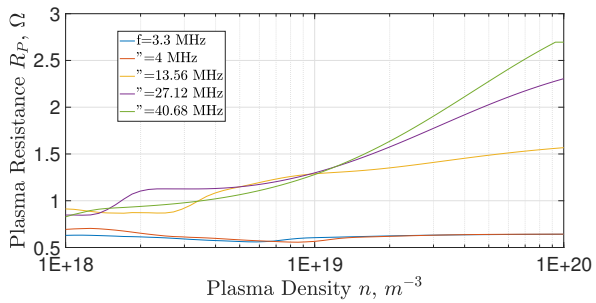

Figure 13: R_P vs n vs f_0, Insulating Top Plate. $\phi = 2a = 37$ mm, $B_0 = 15Gauss$, $m = 1$ Helix 5-turns.

Given the availability at the institute of discharge channel of $\phi = 2a = 37$ mm, we have been focusing on this size, and an Helix antenna of 5 turns $m = 1$ has been applied, as it was observed to provide better performance than the half-helical antecedently applied. Within Fig. 14, 15, 16, and Fig. 17 the effect of variation of f_0 and B_0 is shown. R_P increases and presents sharper profile with increasing f_0 for the given B_0 applied. The frequency variation directly influences the Trivelpiece-Gould wave [15], that is a slow, rapidly damped, electrostatic wave at the boundary where most of the power is coupled. According to [7], R_P increases with f_0 due to TG-damping, as this finally increases with f_0 [7] [16]. TG-wave couples with the helicon mode at the center, therefore for higher f_0, there are larger and wider TG power absorption peaks. Additionally, an advantage of higher frequencies is according to [16] and [17], suggesting that ignition is easier obtained for higher frequencies.

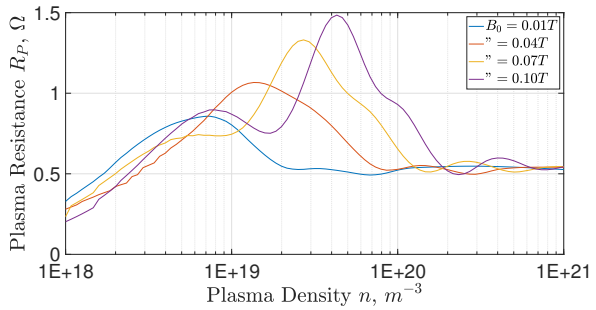

Figure 14: R_P vs n vs B_0, Insulating Top Plate. $\phi = 2a = 37$ mm, $f = 3.3$ MHz, $m = 1$ Helix 5-turns.

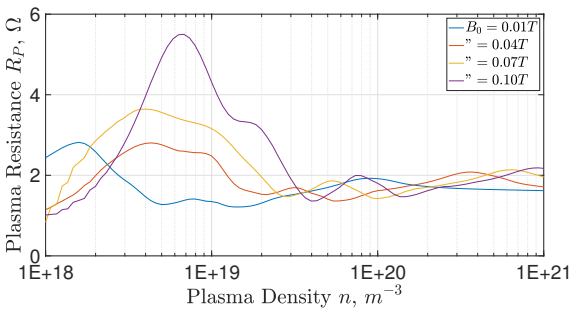

Figure 15: R_P vs n vs B_0, Insulating Top Plate. $\phi = 2a = 37$ mm, $f = 13.56$ MHz, $m = 1$ Helix

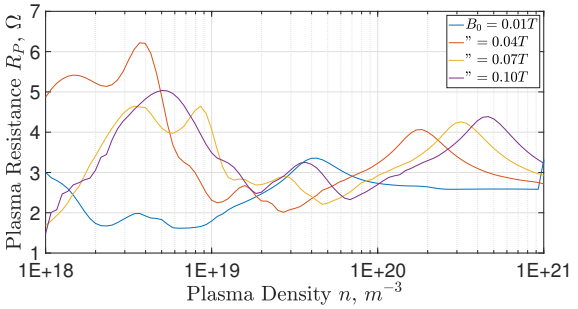

Figure 16: R_P vs n vs B_0, Insulating Top Plate. $\phi = 2a = 37$ mm, $f = 27.12$ MHz, $m = 1$ Helix 5-turns.

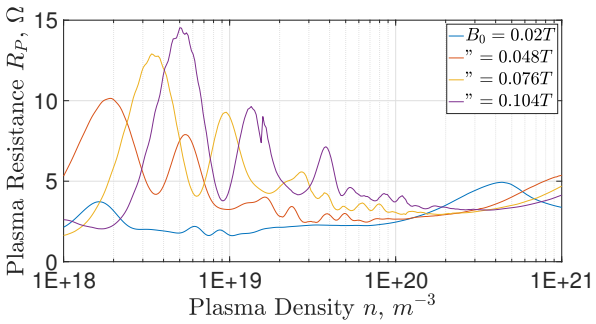

Figure 17: R_P vs n vs B_0, Insulating Top Plate. $\phi = 2a = 37$ mm, $f = 40.68$ MHz, $m = 1$ Helix 5-turns.

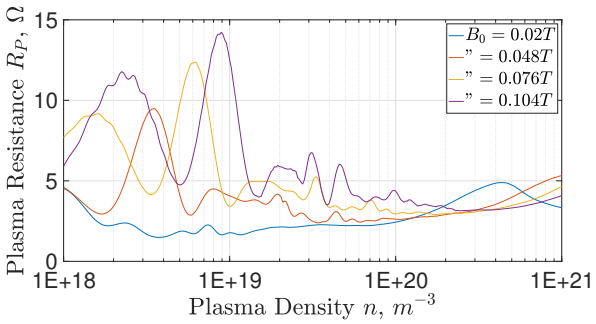

Figure 18: R_P vs n vs B_0, Conducting Top Plate. $\phi = 2a = 37$ mm, $f = 40.68$ MHz, $m = 1$ Helix 5-turns.

Finally, the difference given by the presence of a conductive top plate instead of an insulating one is shown between the Fig. 18 and 17. The low-peak field becomes sharper and a second peak, lower, appears at lower densities, showing a possible wider efficient operating range of the plasma source. This is due to the constructive wave interference caused reflection of the waves by the conducting top plate [7].

6 CONCLUSION

Within this paper the first step into the design of an IPT for ABEP application has been presented. The refurbished facility has been briefly introduced together with the first measurements on the power cooling balance. This serves as test-bed for the development of the ABEP-based IPT. The software tool HELIC is introduced and the input parameters detailed discussed. The results from the simulations allowed to have a better idea on how the main parameters, such as a, f_0, n, B_0, R_P, influences the design of the plasma source for obtaining an efficient discharge. An optimized configuration is possible. Key requirement for the development of the IPT is an efficient plasma discharge. To achieve high exhaust velocities c_e and specific impulse I_{sp}, since the propellant mass flow is limited by the intake [12], [13], [14], electromagnetic acceleration is required. An efficient thrust production requires both efficient ionization and acceleration. Only if the ionization efficiency is high enough, such that the maximum amount of particles can be influenced by the em-fields, and the acceleration efficiency as well, makes possible to accelerate most of the propellant to the required very high c_e for thrust production.

7 OUTLOOK

Finally, a new power supply included an auto-matching network is to be procured given the limitation of the old one, and the assembling of the first step IPT has to begin already in May 2018. This first IPT will be without water cooling, and based on the HELIC simulations for first verification.

8 ACKNOWLEDGEMENTS

This project has received funding from the European Union's Horizon 2020 research and innovation programme under grant agreement No. 737183. This reflects only the author's view and the European Commission is not responsible for any use that may be made of the information it contains.

References

[1] Romano, F., Massuti-Ballester, B., Binder, T., Herdrich, G., Fasoulas, S. & Schönherr, T. (2018). System analysis and test-bed for an atmosphere-breathing electric propulsion system using an inductive plasma thruster, *Acta Astronautica*, **147**, 114 – 126, ISSN 0094-5765, doi:https://doi.org/10.1016/j.actaastro.2018.03.031, URL `http://www.sciencedirect.com/science/article/pii/S009457651730406X`.

[2] Herdrich, G. & Auweter, M. (2006). Inductively heated Plasma Sources for Technical Applications, *Vacuum Journal , Institut für Raumfahrtsysteme (IRS) and Steinbeis Transfer Centre Plasma and Space Technology (STC PRT)*, **80**, 1138–1143.

[3] Dropmann, M., Herdrich, G., Laufer, R., Puckert, D., Fulge, H., Fasoulas, S., Schmoke, J., Cook, M. & Hyde, T.W. (2013). A new inductively driven plasma generator (IPG6)—Setup and initial experiments, *IEEE Transactions on Plasma Science*, **41**(4), 804–810.

[4] Roberts, P.C.E., Crisp, N.H., Edmondson, S., Haigh, S.J., Romano, F., Herdrich, G., Binder, T., Boxberger, A. & Oiko, V.T.A. (09 2017). DISCOVERER – Radical Redesign of Earth Observation Satellites for Sustained Operation at Significantly Lower Altitudes, *International Astronautical Congress 2017, Adelaide, Australia*, **IAC-17-D1,1,2,x41086**.

[5] ESA (May 2005). GOCE System Critical Design Review (CDR), Technical report, ALENIA Spazio.

[6] Romano, F., Herdrich, G., Fasoulas, S. & Schönherr, T. (October 2017). Performance Evaluation of a Novel Inductive

Atmosphere-Breathing EP System, *35th International Electric Propulsion Conference, Atlanta, USA*, **IEPC-2017**(184).

[7] Chen, F.F. (Oct 2008). Permanent Magnet Helicon Source for Ion Propulsion, *IEEE Transactions on Plasma Science*, **36**(5), 2095–2110, ISSN 0093-3813, doi:10.1109/TPS.2008.2004039.

[8] Chen, F.F. (2013). Antenna mechanisms and electrostatic fields in helicon discharges, *Rejected, Plasma Sources Sci. Technol*, p. http://www.ee.ucla.edu/ ffchen/Publs/chen235R.pdf.

[9] Chen, F.F. & Arnush, D. (1997). Generalized theory of helicon waves. I. Normal modes, *Physics of Plasmas*, **4**(9), 3411–3421, doi:10.1063/1.872483, URL `https://doi.org/10.1063/1.872483`.

[10] Arnush, D. & Chen, F.F. (1998). Generalized theory of helicon waves. II. Excitation and absorption, *Physics of Plasmas*, **5**(5), 1239–1254, doi:10.1063/1.872782, URL `https://doi.org/10.1063/1.872782`.

[11] Arnush, D. (2000). The role of Trivelpiece–Gould waves in antenna coupling to helicon waves, *Physics of Plasmas*, **7**(7), 3042–3050, doi:10.1063/1.874157, URL `https://doi.org/10.1063/1.874157`.

[12] Romano, F., Binder, T., Herdrich, G., Fasoulas, S. & Schönherr, T. (July 2015). Air-Intake Design Investigation for an Air-Breathing Electric Propulsion System, *34th International Electric Propulsion Conference, Kobe, Japan*, **IEPC-2015/ISTS-2015-b**(269).

[13] Romano, F., Binder, T., Herdrich, G., Fasoulas, S. & Schönherr, T. (May 2016). Intake Design for an Atmosphere-Breathing Electric Propulsion System, *Space Propulsion 2016, Roma, Italy, 2016*, **SP2016**(3124981).

[14] Binder, T., Boldini, P., Romano, F., Herdrich, G. & Fasoulas, S. (2016). Transmission probabilities of rarefied flows in the application of atmosphere-breathing electric propulsion, *AIP Conference Proceedings*, volume 1786, p. 190011, AIP Publishing, doi:10.1063/1.4967689.

[15] Chen, F.F. & Torreblanca, H. (2006). Helicon discharges and sources: a review, *NSF Final Report*, URL `http://www.seas.ucla.edu/~ffchen/Publs/Chen217R.pdf`.

[16] Chen, F.F. (2015). Helicon discharges and sources: a review, *Plasma Sources Science and Technology*, **24**(1), 014001, URL `http://stacks.iop.org/0963-0252/24/i=1/a=014001`.

[17] Toki, K., Shinohara, S., Tanikawa, T., Funaki, I. & Shamrai, K.P. (2003). Preliminary investigation of helicon plasma source for electric propulsion applications, *Proc. 28th. IEPC*, pp. 1–10.